Microwell-based flow culture reduces hypoxia-induced phenotype and restores drug response in prostate cancer spheroids

Marie C. Payne,[1*] SumYat Ho,[2] Takao Hashimoto,[3,4] Sara Imboden,[1] Brandon S. Lee,[5] Melissa J. Rupert,[5] Nathan Y. Cai,[5] Andrew S. Goldstein,[3,4] and Neil Y.C. Lin[1,5,6]

1 Department of Mechanical & Aerospace Engineering
2 Department of Biochemistry
3 Department of Urology
4 Department of Molecular, Cell & Developmental Biology
5 Department of Bioengineering
6 Institute for Quantitative and Computational Biosciences
University of California, Los Angeles, Los Angeles, CA 90095, USA
* Corresponding author

June 2022

Abstract. 3D cancer spheroids represent a highly promising model for study of cancer progression and therapeutic development. Wide-scale adoption of cancer spheroids, however, remains a challenge due to the lack of control over hypoxic gradients that may cloud the assessment of cell morphology and drug response. Here, we present a Microwell Flow Device (MFD) that generates in-well laminar flow around 3D tissues via repetitive tissue sedimentation. Using a prostate cancer cell line, we demonstrate the spheroids in the MFD exhibit improved cell growth, reduced necrotic core formation, enhanced cellular structure, and down-regulated expression of cell stress genes. The flow-cultured spheroids also exhibit an improved sensitivity to chemotherapy with greater transcriptional response. These results demonstrate how fluidic stimuli reveal the cellular phenotype previously impacted by severe hypoxia. Our platform advances 3D cellular models and enables study into hypoxia modulation, cancer metabolism, and drug screening within pathophysiologically relevant conditions.

Keywords: Cancer Spheroid, Flow Culture, Hypoxia, Drug Response, Prostate Cancer

1. Introduction

3D cancer spheroids are valuable *in vitro* models that have been extensively used in both fundamental research and industrial settings, ranging from precision medicine and drug development to cellular therapies [1, 2]. For example, analysis of cellular growth and migration in *in vitro* cancer spheroids has revealed mechanistic pathways underlying invasive tumor development and metastasis [3, 4]. Studies of multicellular cancer spheroids have also shown that cellular cross-talk plays a role in tumor growth and tumor-mediated immune suppression [5, 6, 7, 8]. More importantly, reconstructing the native 3D architecture has led to greater therapeutic insight into radio- and chemo-sensitivity generated by limited drug penetration and reduced cellular proliferation [9, 10]. In these studies, the 3D spheroids better recapitulate the cell-cell and cell-matrix interactions within tumors compared to traditional 2D monolayer culture. [11, 12, 13]. These interactions closely mimic the complex physical cues found in native tissues and, in turn, lead to *in vivo*-like gene expression profiles and drug responses [14, 15, 16, 17, 18].

Despite such an improved reconstruction of the tumor microenvironment, there is still a substantial discrepancy between 3D culture and primary tumors. A fundamental limitation to 3D spheroids is the development of steep oxygen and metabolite gradients within spheroid cores, leading to necrosis [19, 20, 21]. Solute transport within avascular tissues typically relies on passive diffusion, which restricts nutrient exchange to cells beyond the oxygen diffusion limit of $\sim$100-200 μm [22, 23]. While a well-controlled hypoxic condition in *in vitro* models can be useful to study limited tumor growth, hypoxia-induced cell invasion, drug resistance development, and cellular adaptations to oxidative stress [24, 25, 26, 27], conventional 3D spheroid systems usually exhibit overly severe and physiologically irrelevant levels of necrosis, causing a strongly biased understanding of therapeutic efficacy for three major reasons [28]. First, the sizeable necrosis in large spheroids impacts many essential cellular processes such as the penetration, binding, and bioactivity of therapeutic drugs and drug candidates [29, 30]. Second, most *in vivo* hypoxic conditions are transient, whereas the hypoxic condition in spheroids continuously worsens as the sample grows [19]. Lastly, variations in cell packing and necrotic core size can dominate over cell-specific responses and challenge high-throughput screening accuracy [31, 32]. Identifying solutions for precise control over hypoxic gradients and necrotic formation would greatly improve physiological and clinical relevance in tumor spheroids.

Here, we address challenges of hypoxia-induced necrosis in 3D prostate cancer (PCa) spheroids by developing a fluidic system, the Microwell Flow Device (MFD), that generates laminar flow around spheroids in individual microwells. As demonstrated in other flow culture methods, such as microfluidic devices, bioreactors, and spinner flasks, the external flow can effectively promote intra-tissue transport of oxygen, nutrients, and metabolic wastes [33, 34, 35]. By engineering a gas-permeable and liquid-retaining lid, our MFD repeats 180-degree flipping motion that continually re-suspends spheroids, creating a sustained external flow field through repeated sedimentation caused by

natural density differences ($\sim 10\%$) between biological tissue and surrounding media.

Furthermore, the design of the MFD addresses longstanding challenges of 3D flow culture; in particular, bioreactors and spinner flasks usually demand large quantities of media, generate non-uniform shear stress, and prohibit culture of independent replicates, whereas microfluidic systems require cumbersome fabrication and operation procedures [36, 37]. Our improved and simplified platform is able to administer physiological fluidic stimuli while maintaining throughput and reproducibility of individual replicates. To demonstrate the utility of the MFD culture platform, we generated large (4k cells/well) spheroid models from the Lymph Node Carcinoma of the Prostate (LNCaP) cell line. Large spheroids achieve better physiological relevance in terms of growth, cell function, and drug responses, but have been underutilized in *in vitro* studies due to challenges in viability and long-term growth [38, 39]. We investigate that LNCaP spheroids in the MFD exhibit reduced necrosis and hypoxic stress and maintain cellular structural integrity throughout the spheroid. Modulation of hypoxia in 3D cell culture using the MFD can provide a complimentary model to standard protocols and aid in understanding longitudinal tissue development and drug response dynamics in large ($>$ 1mm) spheroids. Such a dynamic growth environment can prevent the development of toxic, irreversible oxygen gradients which may mask important cell phenotypes [11].

Results

Design of a Microwell Flow Device for Individual, Laminar Flow Culture of Spheroids

To facilitate solute transport in the LNCaP tissues, we designed the MFD to provide uniform shear stress based on spheroid sedimentation. The system is designed to work with commercial well plates and is composed of a custom lid and clamp mechanism that is periodically and consistently rotated by a single stepper motor 180 degrees (Figures 1a and S1). The custom lid is formed by a rigid outer shell, rubber padding, and a 150μm-thick Polydimethylsiloxane (PDMS) membrane (Figure 1b). PDMS is a widely-used silicon-based material that is bio-compatible and simple to fabricate [40] (see Figure S2 for fabrication process). Through its porous structure, the PDMS facilitates this flipping motion by simultaneously retaining liquid and allowing gas exchange to the media. The rate of gas exchange is thickness-dependent, and is comparable to the rate of exchange in an open-diffusion plastic lid (Figures 1c and S3).

Additionally, the MFD addresses limitations of conventional fluidic systems. Compared to a standard 125ml spinner flask or bioreactor, each well in a 96-well plate requires a maximum of 350 μl of media, which is approximately a 3.5-fold reduction in total media consumption. The elimination of mechanical stirrers and tubing resolves unwanted fluidic shear stress gradients, decreases damaging cellular collisions, and reduces labor-intensive culture maintenance [41, 42, 43]. Moreover, by seeding each spheroid in its own well, the samples may be kept biologically independent, providing enhanced statistics and throughput for assays. Using computational fluid dynamics and

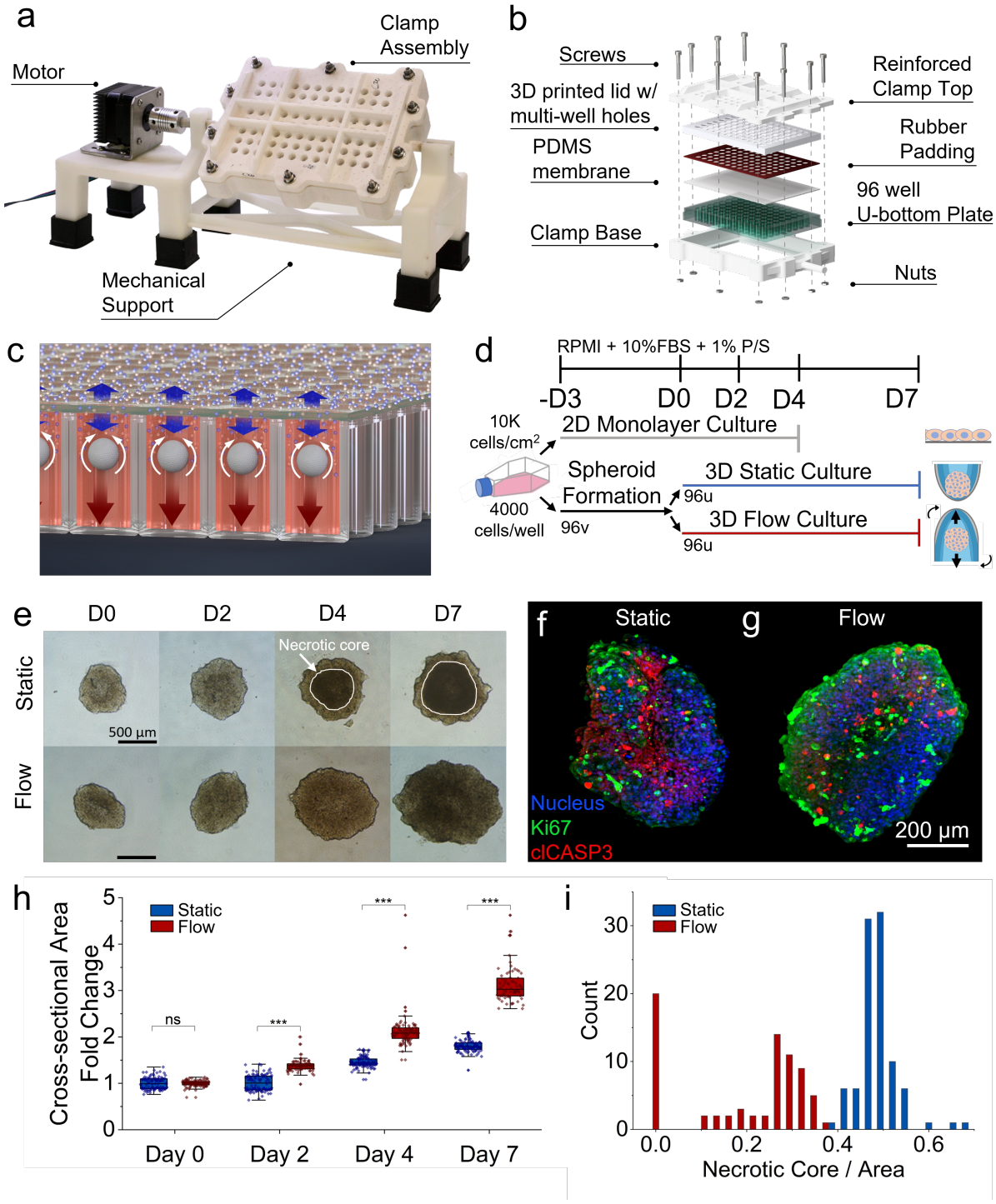

Figure 1: **Microwell fluidic device (MFD) for reducing hypoxic stress in 3D tissues.**

Figure 1: **a** Major components of the MFD include a stepper motor, clamp assembly, and mechanical support. **b** Schematic of the custom clamp design. The custom lid features rubber padding and a 150 μm PDMS membrane to facilitate gas exchange while retaining media. The lid and plate are secured by a 3D printed clamp with 10 exterior screws. **c** Schematic of spheroid motion and gas exchange through the PDMS membrane in individual wells. **d** Timeline of spheroid and 2D monolayer culture. 2D LNCaP cells are grown until 80-100% confluent over ∼4 days. 3D spheroids are aggregated in 96 v-bottom plates for three days and cultured in flow or static conditions until D7. **e** Spheroids are imaged every 2-3 days to quantify morphology changes. By D4, brightfield microscopy images show evidence of a pronounced necrotic core in static culture that is reduced or absent in flow culture. **f-g** Immmunofluorescent imaging of Ki67 and clCASP3 reveals increased cellular proliferation and decreased apoptosis, respectively, in 3DF samples. **h** From brightfield image analysis, spheroids in flow culture grow significantly larger after two days and experience a faster growth rate than static spheroids. **i** Measurements of the necrotic core to cross-sectional area ratio on D7 demonstrate a 30% mean reduction in the necrotic core in flow spheroids (static n = 96; flow n = 73).

Stokesian analysis, we estimate a terminal superficial shear stress of ∼0.16 dynes/cm^2 for a settling spheroid with radius 500μm (Figure S4), which is consistent with physiological values, previous experiments, and experimental measurements [44].

To test how our flow culture device improves the phenotype of 3D human cancer models, we generated spheroids using a metastatic prostate cancer cell line (LNCaP). In brief, the spheroid samples were first generated by seeding 4k cells per well in v-bottom plates to allow the cells to aggregate. After 3 days post-seeding (Day 0) we split the samples into flow (3DF) and static (3DS) conditions and applied flow to the 3DF samples using the MFD for 7 days (Figure 1d). Overall, the 3DF and 3DS samples demonstrate substantially different growth and necrotic core formation (Figure 1e). Immunostaining of Ki67, a marker of cell proliferation, and clCASP3, a marker of cell apoptosis, confirms a strong accumulation of clCASP3 in the static spheroid cores that is largely reduced in the flow samples (Figures 1f-g, Figure S6). Furthermore, the 3DF spheroids exhibited an increased outer proliferative zone, consistent with previous spheroid studies [45, 46]. Measurement of the cross-sectional area validates the significant size differences between the two conditions (Figure 1h). By Day 7, the 3DF spheroids had an average fold increase of 1.5 compared to 3DS, demonstrating high consistency across 4 independent runs (Figure S5). In addition, 3DS spheroids develop a necrotic core that occupies roughly 50% of the total cross-sectional area on Day 7, which was reduced by 30% in the 3DF sample on average (Figure 1i).

We then investigated the importance of continual flow culture by testing the re-emergence of the necrotic core upon flow cessation. To do this, both flow and static spheroids were transferred into static wells on D7 and stained with NucGreen and

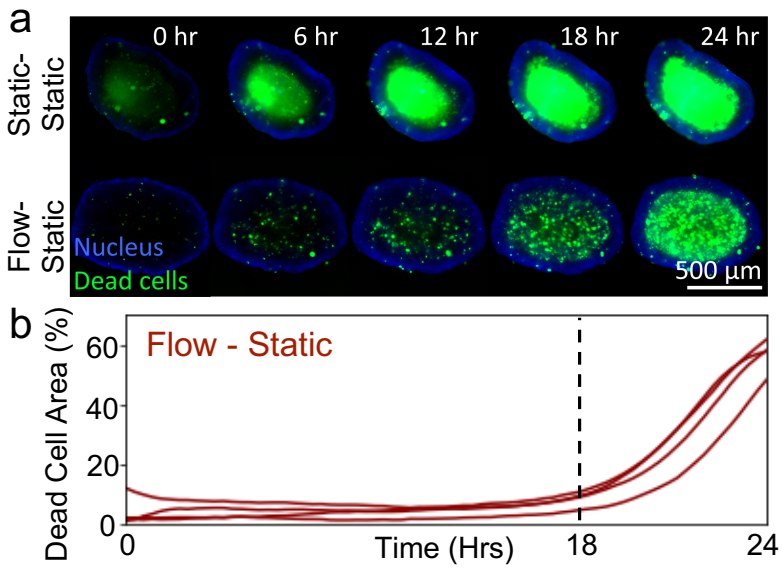

Figure 2: **24hr onset of acute hypoxia after stopping flow. a** Timelapse of live and dead staining for flow and static samples placed in static culture for 24 hours. The flow sample develops a necrotic core starting from 18 hours in static culture. **b** Quantification of dead cell area formation in flow to static spheroids validates the 18-hour timepoint for the onset of acute ischemia.

NucBlue for live/dead imaging (Figures 2a, S7, and Video S1). At roughly 18 hours, the flow-to-static spheroids began to show an increased dead cell quantity throughout the sample core. This 18-hour onset of acute hypoxia was validated by quantifying the dead cell population (Figure 2b). Within 24 hours after being placed in static culture, the flow spheroids appeared visually similar to the static samples, effectively reverting the hypooxia-free phenotype generated by flow.

Flow culture preserves cellular structure and behaviors in LNCaP spheroid cores

To further understand how the applied flow influences the spheroid structure and cellular phenotype, we performed immunostaining of spheroids in both flow and static culture to compare their corresponding morphological phenotypes (Figures 3a-e). We found that the cells in 3DF samples exhibit larger nuclei with greater cell-cell separation compared to the 3DS samples (Figures 3a, d-e). Furthermore, we found that in 3DS samples, only the peripheral cell layers exhibit well-established intercellular junctions with locally enriched E-cadherin (E-cad) expression, whereas the cells in the core show minimal expression with weak local enrichment, indicating compromised intercellular adhesion (Figures 3b-c). In contrast, we observed well-established E-cad junctions in 3DF samples across the entire cross-section. Such a finding suggests that the flow culture uniformly preserves the E-cad-mediated cell-cell interaction, which regulates many cancer-related biological processes such as cell invasion and transdifferentiation [47]. In addition, both

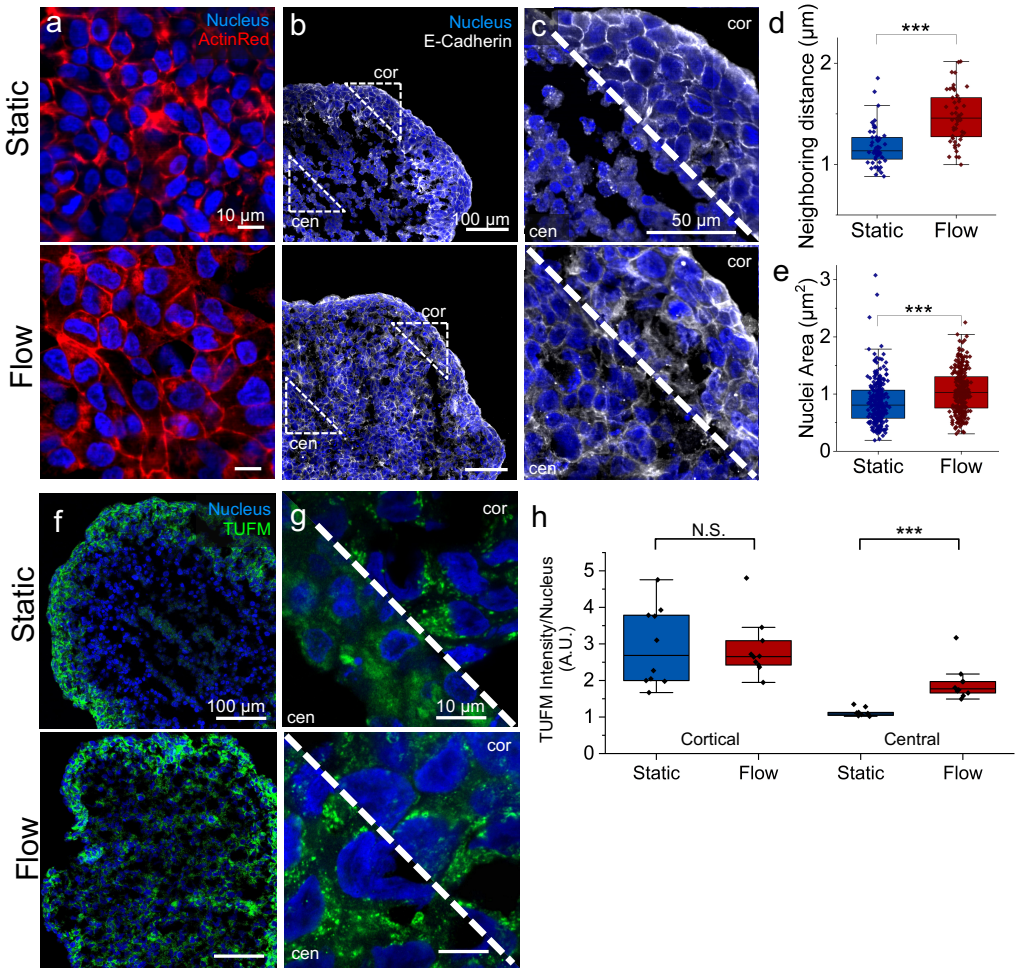

Figure 3: **Immunofluorescent image quantification of 3D and 2D LNCaP cultures.** **a** Sectioned LNCaP spheroids immunostained for cellular filament (ActinRed) and nucleus (Dapi). **b-c** Immunostained LNCaP sections of E-cadherin (E-cad) illustrate cell boundaries. In the cortical areas (cor), flow and static samples appear similar, with strong expression of E-cad present between cells. In the central region (cen), flow maintains structural integrity of E-cad while cells in the static sample experience a breakdown of cellular adhesion. **d** Quantification of distance between neighboring nuclei (Fiji Image J) shows cells in the flow sample are more distant (flow n = 50; static n = 50). **e** Cells in the flow sample additionally exhibit a larger nuclear area (flow n = 275; static n = 268). Significance stars indicate $p<0.001$. **f-g** Immunostaining of TUFM reveals a breakdown in mitochondrial distribution in 3DS cen regions compared to the viable 3DS cor regions. 3DF cen and cor TUFM intensity does not display a visible morphology contrast. **h** Quantification of TUFM intensity per nucleus density. 5 regions of interest were analyzed in Image J in each of the cor and cen regions for flow and static (n=2). The 3DS and 3DF samples exhibit a non-significant cor intensity difference, and a significant ($p<0.001$) reduction in 3DS cen intensity.

3DS and 3DF samples express lipid droplets, FASN, and vimentin (Figure S8), akin to 2D culture (Figure S9). Androgen receptor (AR) and prostate-specific antigen (PSA) are also expressed in both 3D samples without significant difference (Figure S8).

We next characterized the mitochondrial morphology and distribution by immunostaining of TUFM (Tu Translation Elongation Factor, Mitochondrial), a marker of the mitochondrial inner membrane. Between the 3D spheroid cultures, we observed a reduction of TUFM signal in the central area of the 3DS spheroids, whereas 3DF samples exhibited a uniform intensity distribution (Figure 3f). Additionally, the mitochondrial architecture appears spherical or fragmented, characteristic of proliferating cells, across 3DF and in the 3DS cortical region, in contrast to the 3DS central region (Figure 3g). Quantification of the TUFM intensity per nucleus validates the similar mitochondria densities in the 3DS and 3DF cortex versus the central mitochondria loss ($p < 0.001$) in the 3DS samples (Figure 3h).

Flow culture restores hypoxia-induced transcriptional regulation in LNCaP spheroids

To understand the transcriptional response of spheroids under flow, we analyzed the RNA expression level of 45 genes comprising markers of prostate cancer, metabolism, cell viability, and hypoxia (Table S1). By analyzing D7 spheroids, we found that the three culture conditions (i.e., 2DS, 3DS, and 3DF) formed distinct clusters, indicating both the model dimensionality (i.e. 2D vs. 3D) and physiological stimulus (i.e. flow vs. static) impose individual effects on the LNCaP cell behavior (Figure 4a). To highlight the differential gene expression profile induced by the applied flow in the 3D conditions, we generated a volcano plot by normalizing 3DF to 3DS (Figure 4b). Our analysis showed that the flow significantly downregulates hypoxia markers CA9 and CXCR4 by more than 50%. We also observed upregulated expression of SLC1A5, a glutamine transporter, and NDUFA8, a mitochondrial complex-I subunit, which are involved in glutamine metabolism and oxidative phosphorylation [48, 49]. Moreover, we found an inverse differential expression between ENO2, a neuroendocrine marker, and FOLH1, the prostate-specific membrane antigen gene, which indicates a reduced neuroendocrine phenotype in 3DF vs. 3DS [50]. Barcharts of the differential gene expression normalized to the 2D control further illustrate how the gene expression under flow largely recovers back to the baseline expression levels seen in 2D LNCaP models (Figure 4c, Figure S10). These findings collectively suggest that the applied flow mitigates the hypoxia condition and in turn impacts the metabolic and neuroendocrine-like phenotypes of LNCaP cells.

Flow-cultured spheroids enable precise modeling of cellular responses to Docetaxel

The improved phenotype of LNCaP cells in our 3D flow culture allows us to more accurately characterize the drug response that is masked by hypoxia. Here, we perform a dosage response assay using Docetaxel, which is routinely used for treating advanced stages of prostate cancer either alone or in combination with other drugs [51, 52]. We tested four representative concentrations (0, 5, 10 and 20 nMs) by administering

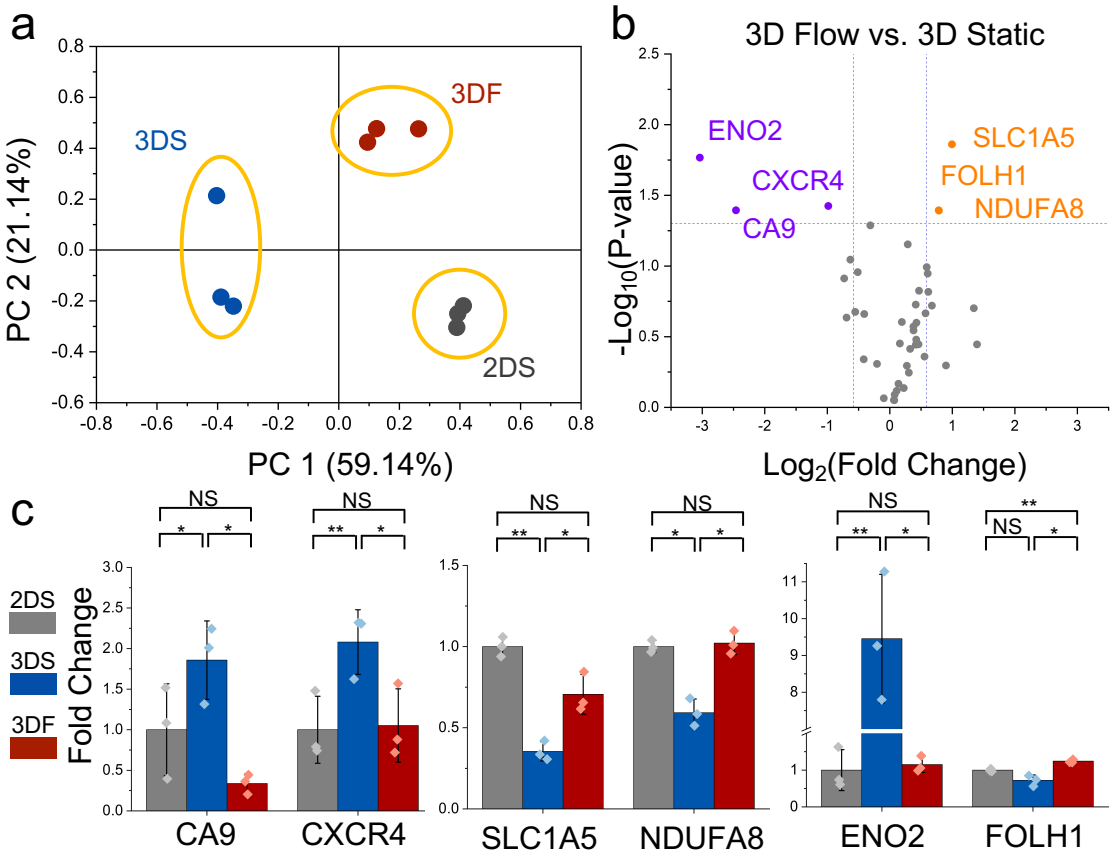

Figure 4: **Gene expression analysis of LNCaP culture conditions.** **a** Principal Component Analysis (PCA) plot of 3D Flow (3DF), 3D Static (3DS), and 2D Static (2DS) culture conditions shows clustering based on normalized gene counts for 45 tested genes. Each data point represents one biological replicate. **b** Volcano plot of upregulated (orange) and downregulated (purple) genes in 3DF condition normalized to 3DS. Significance was determined at $p \leq 0.05$ and fold change ≥ 1.5. **c** Gene expression bar charts of six differentially expressed genes normalized to 2DS. 3DF reverses hypoxic stress seen in 3DS conditions and improves glutamine and mitochondrial activity as measured by increased expression of SLC1A5 and NDUFA8, respectively. A significant upregulation in ENO2 and downregulation in FOLH1 markers in 3DS shows a more neuroendocrine-like phenotype compared to 3DF and 2DS.

Docetaxel to 3DS and 3DF samples on D5 for 48 hours (Figure S11). To visualize dose dependence in the 3D samples, we performed live/dead cell staining (Figure 5a) for the dead cell ratio quantification. Even without the drug applied, the static sample exhibits pronounced cell death due to hypoxia, masking the cell toxicity arising from the Docetaxel treatment. In contrast, the flow culture exhibited a low dead cell baseline in the untreated sample, similar to the 2D control, allowing better characterization of the dosage response (Figure S12). Such a finding is confirmed by quantifying the ratio

of live to dead cells between 3DS and 3DF (Figure 5b).

We also found that the 3DF and 3DS samples exhibit drastically different spatial distributions of dead cells. In static culture, the central necrosis intensifies at higher concentrations of Docetaxel and spreads outwards, whereas the flow sample begins to express cell death at the periphery and develops a uniform expression throughout the spheroid. Such a contrast can be visualized by averaging the NucGreen intensity (i.e. dead cell) radially outwards from the spheroid center (Figure 5c), in which the static samples show a steep intensity gradient with the most death present at the core while the flow samples show a relatively flat intensity. Our cell viability analysis illustrates the importance of intra-tissue solute transport for uncovering potential confounders in toxicity assays.

To further understand how the culture condition impacts the cellular response to drug treatment, we visualized corresponding gene expression changes in 10nM Docetaxel treated vs. untreated samples using volcano plots (Figure 5d). Compared to the 2DS and 3DS samples, the 3DF spheroids reveal a more substantial transcriptional change. A total of 17 genes were significantly down- or upregulated due to the Docetaxel treatment in the 3DF sample, whereas the 3DS and 2DS conditions only display 3 genes. To identify the effect of flow on Docetaxel-induced transcriptional response, we generated a comparison of the gene expression fold change between treated and untreated conditions in flow and static (Figure 5e). This analysis shows that the Docetaxel treatment upregulates essential hypoxia (i.e. CA9, CXCR4, and HMOX1) and neuroendocrine (i.e. ENO2) markers in the flow sample. This result, however, is masked in the static sample, since these hypoxia-related markers readily exhibit a high baseline expression level in untreated spheroids. Together, our results suggest accurate interpretations of cell response to drug treatment heavily relies on physiologically relevant growth conditions. Our flow-cultured samples address a number of limitations of 3D cell models, primarily by mitigating the hypoxic condition within 3D samples.

Discussion & Conclusions

3D tissues better recapitulate *in-vivo* tissue growth and therapeutic response compared to 2D culture, however there are technical hurdles that prevent widespread adoption. First, the insufficient solute transport causes overwhelming hypoxia-induced necrosis in the core of spheroids, generating steep metabolite and oxygen gradients across the sample, clouding the assessment of cell phenotype and drug response [53, 54]. In this study, we report a Microwell Flow Device (MFD), a scalable system that generates physiologically-relevant fluidic stimuli that drives nutrients toward the tissue core, which in turn maintains central tissue structure and cellular behaviors. Overall, our system generates laminar flow and individual replicates, two qualities that have been difficult to achieve simultaneously in 3D flow culture. The MFD can be tailored to any plate dimension and, in future work, may be scaled up to accommodate mid-throughput (>1000 sample) assays. These properties serve to improve tissue quality and uniformity

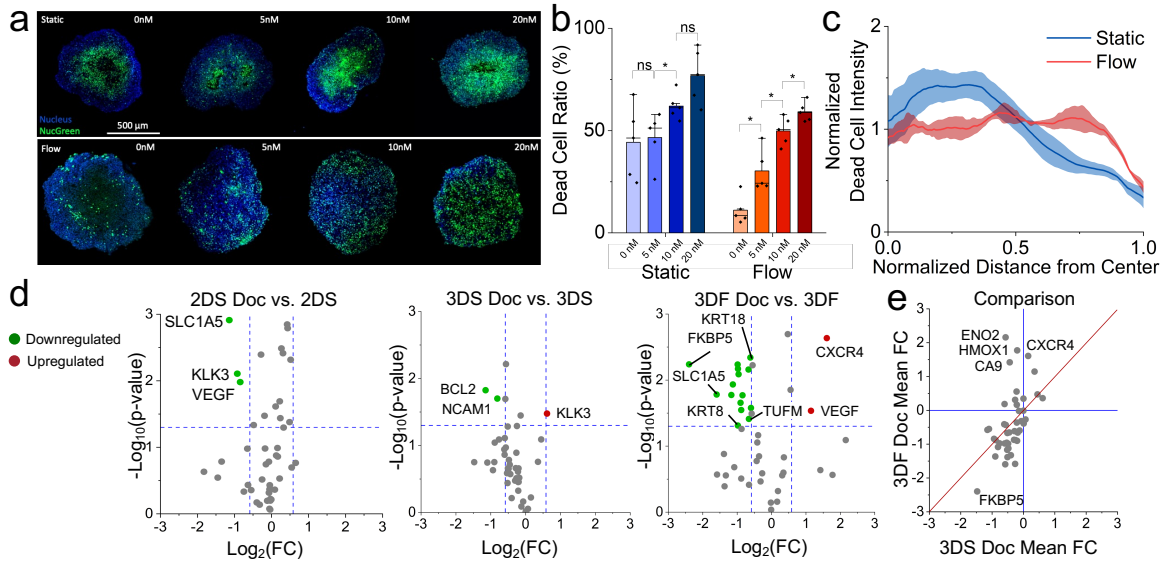

Figure 5: **Differential gene expression of Docetaxel in static vs. flow cultured spheroids.** **a** Dose response of static and flow spheroids for 0, 5, 10 and 20nM concentrations of Docetaxel. Static spheroids display necrosis prior to drug administration and localized cell death at the core at all drug concentrations. In contrast, flow spheroids display a more uniform expression of cell death. **b** Measurement of the ratio of dead cells to the entire spheroid area. 3DF samples show increased sensitivity to varying drug concentrations (static n = 5; flow n = 5). **c** Quantification of cell death by radial integration of dead cell count from the center to the perimeter of the spheroid. Flow spheroids show less cell death in the center and a more uniform expression from the center to edge. **d** Volcano plots of 2DS, 3DS and 3DF differential gene expression for treated samples normalized to corresponding untreated samples. Red dots are upregulated after treatment with 10nM Docetaxel and green are downregulated after treatment. Significance was determined at $p \leq 0.05$ and fold change ≥ 1.5. Each assay was performed in triplicate. **e** Comparison of mean fold change between 3DS and 3DF treated vs. untreated samples. Genes in the second quadrant indicate upregulation in flow samples and downregulation in static samples post treatment.

as well as compatibility with high-throughput screening platforms, thereby encouraging use of 3D tissue models for both basic research and therapeutic development.

As demonstrated in LNCaP spheroids, flow-cultured samples are able to grow larger for longer periods of time without excessive central necrosis. On the cellular level, we observed reduced hypoxia-induced apoptosis throughout the spheroid and increased cellular proliferation near the sample periphery. Immunofluorescence microscopy reveals restoration of cell packing, intercellular adhesion, and mitochondrial morphology in flow samples. Furthermore, we commonly observed a lack of immunofluorescent expression in the core of static samples, likely affected by hypoxia and cellular necrosis. This observed expression pattern may skew interpretation of experimental readouts, such as

bulk analyses like Western Blot. Furthermore, our gene expression measurement shows that the applied flow reverts the expression of hypoxia, metabolic, and neuroendocrine-related markers that were altered in conventional static culture. Lastly, the flow culture model exhibits increased sensitivity to Docetaxel, with a uniform cell death distribution and higher differential transcriptional response. This finding is consistent with previous studies which suggest that removing hypoxia-induced cellular drug resistance could increase the cellular response to chemotherapy [55, 56, 57], and which show flow culture-derived spheroids can show reduced sensitivity compared to 2D models [58].

Our culture platform further provides a foundation for mechanistically investigating longstanding questions in PCa metabolism. Metabolic activity in cancer cells plays a pivotal role in tumor growth, metastasis, and drug response. [25, 59, 56]. However, traditional 3D static culture often exhibits a metabolic phenotype that is strongly affected by hypoxia, potentially skewing experimental readouts. As shown in this work, our MFD effectively restores the cellular behavior in 3D spheroids, providing an improved platform for metabolic assays. The MFD could also be used for long-term study of metabolic shifts in thick (>1mm) tissues without significant necrosis. In addition, our system allows the modulation of the hypoxic onset, which opens the door for modeling acute ischemia and temporal oxygen availability on cellular metabolism and drug response.

By increasing the complexity of the spheroid microenviroment, such as co-culture with stromal cells or implementation of circulating tumor cells, our culture system can enable future studies that provide critical insights into intercellular signaling and how it dictates tumor remodeling and cell invasion. Similarly, vascularized multicellular spheroids, organoids, and patient-derived explants, which have been shown to exhibit *in vivo*-like structure and function [60], can be directly implemented in our platform to better recapitulate the responses akin to native tissue. By growing independent replicates, our culture device provides an unprecedented and scalable platform to conduct mid to large-scale screening of compounds and signaling factors, accelerating developments of combinatorial therapy and precision medicine.

2. Methods

MFD Manufacturing All components of the MFD were 3D printed (Formlabs Form 3). The custom 96 well plate lid consisted of a PDMS membrane and a laser-cut silicone rubber sheet (McMaster-Carr, 9010K11) adhered to the lid using silicone sealant (Loctite, 908570). For the PDMS membrane, 10g of Sylgard 184 (Dow Corning, 11-3184-01 C) was mixed with a 10:1 monomer:catalyst ratio, spin coated to a thickness of 150μm, and cured at 150^{o}C for 35 minutes. Prior to use, all lid components were sterilized by soaking in 70% ethanol for a minimum of 10 minutes before use and air dried. Device rotation was controlled by a NEMA 17 stepper motor connected to an A4988 stepper motor driver and Arduino UNO microcontroller, programmed to flip 180^o every 10 seconds.

Cell Culture Human prostate adenocarcinoma-derived LNCaPs were cultured according to the ATCC thawing, propagating, and cryopreserving protocol [61, 62]. The culture media for LNCaP comprised of RPMI 1640 (Gibco), 10% fetal bovine serum (Gibco), and 1% Penicillin/ Streptomycin (Gibco). LNCaP culture was incubated at 37°C, 5% CO2, and 90% relative humidity. Media change was performed every 24 to 48 hours. Subculture of LNCaPs was performed at $\sim$ 80% confluency, in which the cells were washed with 1X PBS -/- twice, and incubated with 0.5% Trypsin-EDTA at 37°C for cell detachment. The dissociated cells were then centrifuged at 250g for 3 minutes, and re-suspended in warmed culture media. In 2D culture, the seeding density was 10,000 cells/cm^2 on poly-l-sine (Sigma-Aldrich) coated surface. For 3D culture, LNCaPs were seeded into Greiner Bio-One™ CellStar™ 96-Well, Cell Repellent-Treated, V-Shaped-Bottom Microplate at 4K cells/well. For better aggregation of LNCaP, the 96-well plate is centrifuged at 300g for 10 minutes. Before introduction of the flow or drug conditions, the spheroids were allowed to grow for 72 hours post seeding. For experiments, LNCaP spheroids were transferred into Corning 96 Well Clear Ultra Low Attachment Microplates. To monitor the growth of monolayer and spheroid culture, phase contrast images were taken right after media change on an Olympus CKX41 at 4x magnification.

Spheroid Sectioning & Immunofluorescent Imaging Spheroids for cryosectioning were fixed in 4% Paraformaldehyde (PFA) in Phosphate Buffered Saline (PBS +/+) for 20 minutes on ice and then washed three times in PBS +/+. Spheroids were then placed in 30% sucrose in PBS +/+ for 1-3 hours on ice until completely submersed. The spheroids were embedded and frozen in Tissue-Tek Optimal Cutting Temperature (O.C.T., Sakura) compound, cryosectioned at 12μm thickness, and collected onto Superfrost Plus slides (Fisher Scientific).

The LNCaP samples were first blocked using a mixture of 2% donkey serum (Sigma-Aldrich, D9663-10ML) and 0.5% Triton X-100 (Sigma-Aldrich, T8787-50ML) in PBS +/+ for 30 minutes (2D) or 60 minutes (whole & cryosectioned spheroids). After blocking, the slides were washed with PBS twice, and then incubated with the primary staining solution (0.5% BSA, 0.25% Triton X-100, and the primary antibody (SI Table 2)). The samples were left in the staining solution for 30 minutes (2D), overnight (cryosectioned slides), or for 24 hours (whole spheroids), followed by two washes with 1X PBS. Afterwards, the secondary staining solution (with NucBlue and the secondary antibody (SI Table 2)) was added for 30 minutes (2D), 60 minutes (cryosectioned spheroids), or 24 hours (whole spheroids). 2D and whole mount spheroids were washed twice with PBS and stored in 0.1% Tween 20 (Sigma-Aldrich, P9416-50ML) at 4^{o}C. Sectioned slides were mounted with cover slips using Prolong Diamond antifade mountant (Thermo Fisher Scientific, P36970) and stored at 4^{o}C.

Gene Expression Measurements To prepare 3D LNCaP spheroids for RNA extraction, 30 spheroids/biological replicate of 3DS and 10 spheroids/biological replicate of 3DF

were collected in triplicate and washed twice with PBS +/+ (Gibco). For 2D LNCaP culture, samples were washed twice with PBS +/+. LNCaP samples were lyzed with the TRI Reagent (ZYMO Research). RNA extraction is then performed using the Direct-zolTM RNA MiniPrep Plus kit (ZYMO Research). Quality and Concentration of the extracted RNA solution were assessed with Thermo Scientific™ NanoDrop™ 2000/2000c Spectrophotometers. Triplicate RNA samples from each condition were diluted to 20 ng/μl with DNase/RNase-Free Water (ZYMO RESEARCH). 15μl RNA solution of each replicate were sent to the UCLA Center for Systems Biomedicine for RNA expression assay with the Nanostring™ nCounter. Expression of 45 genes related to metabolic pathway, androgen receptor signaling, hypoxia, viability, are neuroendocrine differentiation were analyzed. The results was normalized with gene expression of three housekeeping genes. Consistency of triplicates was assessed by Principal Component Analysis in Origin Pro software. The results of the gene expression measurements are visualized with volcano plots (Origin Pro).

Transmitted Light Microscopy and Fluorescent Imaging All stained LNCaP samples, shown in figures 1 and 3, were imaged using an Confocal microscope with a 10x or 40x objective. Cell viability images (figures 2 and 5) were acquired with an inverted microscope (Etaluma LS720) with a 4x phase contrast objective (Olympus, CACHN10XIPC) inside an incubator. For each well of the 96 wells, one image for each channel (i.e., phase contrast, 405 nm, and 488 nm) was obtained with a field of view $\sim 770\mu$m$\times 770\mu$m. To conduct the time-lapse experiment, every well was imaged every 20 minutes over a period of 48 hours. While all of our selected antibodies have been previously validated, we also examined the non-specific binding by measuring the fluorescent intensity in samples that were only stained with secondary antibodies. Prior to further analyses, the background of the fluorescent data was evaluated and subtracted. Image analysis was performed using Fiji Image J.

Statistical Analysis Data are reported as mean values $\pm$ standard deviation (SD). Statistical analysis was performed using Microsoft Excel, and statistical significance was determined using 2-tailed paired t-tests. Significance levels are indicated with asterisks in each figure caption. P values ≤ 0.05, 0.01, and 0.001 are indicated with one, two, or three asterisks, respectively. PCA was performed in Origin Pro.

Acknowledgments

Funding: This work was funded by the Broad Stem Cell Research Center at the University of California, Los Angeles and the UCLA SPORE in Prostate Cancer Grant (P50 CA092131). This material is also based upon work supported by the National Science Foundation Graduate Research Fellowship under Grant No. DGE-2034835.
We are grateful to Dorian Luccioni for assistance in the engineering renderings.

Author Contributions: M.-C.P., A.-S.G., and N.-Y.C.L. designed the project. M.-C.P., A.-S.G., and N.-Y.C. L. wrote the manuscript. M.-C.P., S.H., T.H., S.I., B.-S.L., M.-J.R., and N.-Y.C. performed the experiments. M.-C.P., T.H., S.I., M.-J.R., and N.-Y.C. analyzed the data. M.R. performed RNA extraction. T.H. and A.-S.G. provided the LNCaP cells. All authors reviewed and approved the manuscript.

Competing Interests: The authors declare that they have no competing interests.

Supplementary materials

Figures S1 through S12
Tables S1 & S2
Captions for Video S1
Supplementary Video S1

3. Bibliography

[1] Eelco Fennema, Nicolas Rivron, Jeroen Rouwkema, Clemens van Blitterswijk, and Jan De Boer. Spheroid culture as a tool for creating 3d complex tissues. *Trends in biotechnology*, 31(2):108–115, 2013.

[2] Juergen Friedrich, Claudia Seidel, Reinhard Ebner, and Leoni A Kunz-Schughart. Spheroid-based drug screen: considerations and practical approach. *Nature protocols*, 4(3):309–324, 2009.

[3] Ville Härmä, Johannes Virtanen, Rami Mäkelä, Antti Happonen, John-Patrick Mpindi, Matias Knuuttila, Pekka Kohonen, Jyrki Lötjönen, Olli Kallioniemi, and Matthias Nees. A comprehensive panel of three-dimensional models for studies of prostate cancer growth, invasion and drug responses. *PloS one*, 5(5):e10431, 2010.

[4] Kristy Shield, M Leigh Ackland, Nuzhat Ahmed, and Gregory E Rice. Multicellular spheroids in ovarian cancer metastases: Biology and pathology. *Gynecologic oncology*, 113(1):143–148, 2009.

[5] Gianpiero Lazzari, Valérie Nicolas, Michiya Matsusaki, Mitsuru Akashi, Patrick Couvreur, and Simona Mura. Multicellular spheroid based on a triple co-culture: A novel 3d model to mimic pancreatic tumor complexity. *Acta biomaterialia*, 78:296–307, 2018.

[6] Amy Y Hsiao, Yu-suke Torisawa, Yi-Chung Tung, Sudha Sud, Russell S Taichman, Kenneth J Pienta, and Shuichi Takayama. Microfluidic system for formation of pc-3 prostate cancer co-culture spheroids. *Biomaterials*, 30(16):3020–3027, 2009.

[7] Janina Kuen, Diana Darowski, Tobias Kluge, and Meher Majety. Pancreatic cancer cell/fibroblast co-culture induces m2 like macrophages that influence therapeutic response in a 3d model. *PloS one*, 12(7):e0182039, 2017.

[8] Tristan Courau, Julie Bonnereau, Justine Chicoteau, Hugo Bottois, Romain Remark, Laura Assante Miranda, Antoine Toubert, Mathieu Blery, Thomas Aparicio, Matthieu Allez, et al. Cocultures of human colorectal tumor spheroids with immune cells reveal the therapeutic potential of mica/b and nkg2a targeting for cancer treatment. *Journal for immunotherapy of cancer*, 7(1):1–14, 2019.

[9] Andrea Frankel, Shan Man, Peter Elliott, Julian Adams, and Robert S Kerbel. Lack of multicellular drug resistance observed in human ovarian and prostate carcinoma treated with the proteasome inhibitor ps-341. *Clinical Cancer Research*, 6(9):3719–3728, 2000.

[10] Åse M Ballangrud, Wei-Hong Yang, David E Charlton, Michael R McDevitt, Klaus A Hamacher, Katherine S Panageas, Dangshe Ma, Neil H Bander, David A Scheinberg, and George Sgouros. Response of lncap spheroids after treatment with an α-particle emitter (213bi)-labeled anti-prostate-specific membrane antigen antibody (j591). *Cancer research*, 61(5):2008–2014, 2001.

[11] Linda G Griffith and Melody A Swartz. Capturing complex 3d tissue physiology in vitro. *Nature reviews Molecular cell biology*, 7(3):211–224, 2006.

[12] Susan Breslin and Lorraine O'Driscoll. Three-dimensional cell culture: the missing link in drug discovery. *Drug discovery today*, 18(5-6):240–249, 2013.

[13] Elisabete C Costa, André F Moreira, Duarte de Melo-Diogo, Vítor M Gaspar, Marco P Carvalho, and Ilídio J Correia. 3d tumor spheroids: an overview on the tools and techniques used for their analysis. *Biotechnology advances*, 34(8):1427–1441, 2016.

[14] Jong Bin Kim. Three-dimensional tissue culture models in cancer biology. In *Seminars in cancer biology*, volume 15, pages 365–377. Elsevier, 2005.

[15] A C Luca, S Mersch, R Deenen, S Schmidt, and I Messner. Impact of the 3d microenvironment on phenotype, gene expression, and egfr inhibition of colorectal cancer cell lines. *PLoS ONE*, 8:59689, 2013.

[16] Kayla Duval, Hannah Grover, Li-Hsin Han, Yongchao Mou, Adrian F Pegoraro, Jeffery Fredberg, and Zi Chen. Modeling physiological events in 2d vs. 3d cell culture. *Physiology*, 32(4):266–277, 2017.

[17] Rasheena Edmondson, Jessica Jenkins Broglie, Audrey F Adcock, and Liju Yang. Three-dimensional cell culture systems and their applications in drug discovery and cell-based

biosensors. *Assay and drug development technologies*, 12(4):207–218, 2014.

[18] AW Stoker, CH Streuli, M Martins-Green, and MJ Bissell. Designer microenvironments for the analysis of cell and tissue function. *Current opinion in cell biology*, 2(5):864–874, 1990.

[19] W Mueller-Klieser, JP Freyer, and RM Sutherland. Influence of glucose and oxygen supply conditions on the oxygenation of multicellular spheroids. *British journal of cancer*, 53(3):345–353, 1986.

[20] James P Freyer and Robert M Sutherland. Regulation of growth saturation and development of necrosis in emt6/ro multicellular spheroids by the glucose and oxygen supply. *Cancer research*, 46(7):3504–3512, 1986.

[21] Raja Venkatasubramanian, Michael A Henson, and Neil S Forbes. Incorporating energy metabolism into a growth model of multicellular tumor spheroids. *Journal of theoretical biology*, 242(2):440–453, 2006.

[22] Min Hee Kim, Steven D Green, Chien-Chi Lin, and Heiko Konig. Engineering tools for regulating hypoxia in tumour models. *Journal of Cellular and Molecular Medicine*, 25(16):7581–7592, 2021.

[23] Peggy L Olive, Charlene Vikse, and Martin J Trotter. Measurement of oxygen diffusion distance in tumor cubes using a fluorescent hypoxia probe. *International Journal of Radiation Oncology* Biology* Physics*, 22(3):397–402, 1992.

[24] Stephen Riffle and Rashmi S Hegde. Modeling tumor cell adaptations to hypoxia in multicellular tumor spheroids. *Journal of Experimental & Clinical Cancer Research*, 36(1):1–10, 2017.

[25] Sara Rodríguez-Enríquez, Juan Carlos Gallardo-Pérez, Alejandro Avilés-Salas, Alvaro Marín-Hernández, Liliana Carreño-Fuentes, Vilma Maldonado-Lagunas, and Rafael Moreno-Sánchez. Energy metabolism transition in multi-cellular human tumor spheroids. *Journal of cellular physiology*, 216(1):189–197, 2008.

[26] EM Hammond, M-C Asselin, Duncan Forster, James PB O'Connor, JM Senra, and KJ Williams. The meaning, measurement and modification of hypoxia in the laboratory and the clinic. *Clinical oncology*, 26(5):277–288, 2014.

[27] Geeta Mehta, Amy Y Hsiao, Marylou Ingram, Gary D Luker, and Shuichi Takayama. Opportunities and challenges for use of tumor spheroids as models to test drug delivery and efficacy. *Journal of controlled release*, 164(2):192–204, 2012.

[28] Peter Vaupel and Arnulf Mayer. Hypoxia in cancer: significance and impact on clinical outcome. *Cancer and Metastasis Reviews*, 26(2):225–239, 2007.

[29] Franziska Hirschhaeuser, Heike Menne, Claudia Dittfeld, Jonathan West, Wolfgang Mueller-Klieser, and Leoni A Kunz-Schughart. Multicellular tumor spheroids: an underestimated tool is catching up again. *Journal of biotechnology*, 148(1):3–15, 2010.

[30] Moriah E Katt, Amanda L Placone, Andrew D Wong, Zinnia S Xu, and Peter C Searson. In vitro tumor models: advantages, disadvantages, variables, and selecting the right platform. *Frontiers in bioengineering and biotechnology*, 4:12, 2016.

[31] Se Jik Han, Sangwoo Kwon, and Kyung Sook Kim. Challenges of applying multicellular tumor spheroids in preclinical phase. *Cancer Cell International*, 21(1):1–19, 2021.

[32] Frédérique Mittler, Patricia Obeïd, Anastasia V Rulina, Vincent Haguet, Xavier Gidrol, and Maxim Y Balakirev. High-content monitoring of drug effects in a 3d spheroid model. *Frontiers in oncology*, 7:293, 2017.

[33] Ruei-Zhen Lin and Hwan-You Chang. Recent advances in three-dimensional multicellular spheroid culture for biomedical research. *Biotechnology Journal: Healthcare Nutrition Technology*, 3(9-10):1172–1184, 2008.

[34] Yves Martin and Patrick Vermette. Bioreactors for tissue mass culture: design, characterization, and recent advances. *Biomaterials*, 26(35):7481–7503, 2005.

[35] Donald E. Ingber. Human organs-on-chips for disease modelling, drug development and personalized medicine. *Nature Reviews Genetics*, 23(1):1–25, 2022.

[36] Koh Meng Aw Yong, Zida Li, Sofia D Merajver, and Jianping Fu. Tracking the tumor invasion

front using long-term fluidic tumoroid culture. *Scientific reports*, 7(1):1–7, 2017.

[37] John A Hickman, Ralph Graeser, Ronald de Hoogt, Suzana Vidic, Catarina Brito, Matthias Gutekunst, and Heiko van der Kuip. Three-dimensional models of cancer for pharmacology and cancer cell biology: capturing tumor complexity in vitro/ex vivo. *Biotechnology journal*, 9(9):1115–1128, 2014.

[38] Mona Mansouri, Samantha Beemer, Chandrasekhar R Kothapalli, Tyler Rhoades, Petru S Fodor, Dola Das, and Nic D Leipzig. Generation of oxygenating fluorinated methacrylamide chitosan microparticles to increase cell survival and function in large liver spheroids. *ACS Applied Materials & Interfaces*, 2022.

[39] Guocheng Fang, Hongxu Lu, Andrew Law, David Gallego-Ortega, Dayong Jin, and Gungun Lin. Gradient-sized control of tumor spheroids on a single chip. *Lab on a Chip*, 19(24):4093–4103, 2019.

[40] Marie-Claire Bélanger and Yves Marois. Hemocompatibility, biocompatibility, inflammatory and in vivo studies of primary reference materials low-density polyethylene and polydimethylsiloxane: A review. *Journal of Biomedical Materials Research: An Official Journal of The Society for Biomaterials, The Japanese Society for Biomaterials, and The Australian Society for Biomaterials and the Korean Society for Biomaterials*, 58(5):467–477, 2001.

[41] Philippe Sucosky, Diego F Osorio, Jason B Brown, and G Paul Neitzel. Fluid mechanics of a spinner-flask bioreactor. *Biotechnology and bioengineering*, 85(1):34–46, 2004.

[42] Masoud Ghasemian, Carys Layton, Daniel Nampe, Nicole Isolde zur Nieden, Hideaki Tsutsui, and Marko Princevac. Hydrodynamic characterization within a spinner flask and a rotary wall vessel for stem cell culture. *Biochemical Engineering Journal*, 157:107533, 2020.

[43] Robert S Cherry and Eleftherios Terry Papoutsakis. Physical mechanisms of cell damage in microcarrier cell culture bioreactors. *Biotechnology and bioengineering*, 32(8):1001–1014, 1988.

[44] Emily J Ross, Emily R Gordon, Hanna Sothers, Roshan Darji, Oakley Baron, Dustin Haithcock, Balabhaskar Prabhakarpandian, Kapil Pant, Richard M Myers, Sara J Cooper, et al. Three dimensional modeling of biologically relevant fluid shear stress in human renal tubule cells mimics in vivo transcriptional profiles. *Scientific Reports*, 11(1):1–14, 2021.

[45] Karolin Froehlich, Jan-Dirk Haeger, Julia Heger, Jana Pastuschek, Stella Mary Photini, Yan Yan, Amelie Lupp, Christiane Pfarrer, Ralf Mrowka, Ekkehard Schleußner, et al. Generation of multicellular breast cancer tumor spheroids: comparison of different protocols. *Journal of mammary gland biology and neoplasia*, 21(3):89–98, 2016.

[46] Hong Song, Odile David, Sanda Clejan, Carrie L Giordano, Helena Pappas-Lebeau, Li Xu, and Kim C O'connor. Spatial composition of prostate cancer spheroids in mixed and static cultures. *Tissue engineering*, 10(7-8):1266–1276, 2004.

[47] Sonia How Ming Wong, Chee Mun Fang, Lay-Hong Chuah, Chee Onn Leong, and Siew Ching Ngai. E-cadherin: Its dysregulation in carcinogenesis and clinical implications. *Critical reviews in oncology/hematology*, 121:11–22, 2018.

[48] Mark A White, Chenchu Lin, Kimal Rajapakshe, Jianrong Dong, Yan Shi, Efrosini Tsouko, Ratna Mukhopadhyay, Diana Jasso, Wajahat Dawood, Cristian Coarfa, et al. Glutamine transporters are targets of multiple oncogenic signaling pathways in prostate cancer. *Molecular Cancer Research*, 15(8):1017–1028, 2017.

[49] Qian Wang, Rae-Anne Hardie, Andrew J Hoy, Michelle Van Geldermalsen, Dadi Gao, Ladan Fazli, Martin C Sadowski, Seher Balaban, Mark Schreuder, Rajini Nagarajah, et al. Targeting asct2-mediated glutamine uptake blocks prostate cancer growth and tumour development. *The Journal of pathology*, 236(3):278–289, 2015.

[50] Martin K Bakht, Iulian Derecichei, Yinan Li, Rosa-Maria Ferraiuolo, Mark Dunning, So Won Oh, Abdulkadir Hussein, Hyewon Youn, Keith F Stringer, Chang Wook Jeong, et al. Neuroendocrine differentiation of prostate cancer leads to psma suppression. *Endocrine-related cancer*, 26(2):131–146, 2019.

[51] Daniel P Petrylak, Catherine M Tangen, Maha HA Hussain, Primo N Lara Jr, Jeffrey A Jones,

Mary Ellen Taplin, Patrick A Burch, Donna Berry, Carol Moinpour, Manish Kohli, et al. Docetaxel and estramustine compared with mitoxantrone and prednisone for advanced refractory prostate cancer. *New England Journal of Medicine*, 351(15):1513–1520, 2004.

[52] Ian F Tannock, Ronald De Wit, William R Berry, Jozsef Horti, Anna Pluzanska, Kim N Chi, Stephane Oudard, Christine Théodore, Nicholas D James, Ingela Turesson, et al. Docetaxel plus prednisone or mitoxantrone plus prednisone for advanced prostate cancer. *New England Journal of Medicine*, 351(15):1502–1512, 2004.

[53] Maria Vinci, Sharon Gowan, Frances Boxall, Lisa Patterson, Miriam Zimmermann, Cara Lomas, Marta Mendiola, David Hardisson, Suzanne A Eccles, et al. Advances in establishment and analysis of three-dimensional tumor spheroid-based functional assays for target validation and drug evaluation. *BMC biology*, 10(1):1–21, 2012.

[54] Michele Zanoni, Filippo Piccinini, Chiara Arienti, Alice Zamagni, Spartaco Santi, Rolando Polico, Alessandro Bevilacqua, and Anna Tesei. 3d tumor spheroid models for in vitro therapeutic screening: a systematic approach to enhance the biological relevance of data obtained. *Scientific reports*, 6(1):1–11, 2016.

[55] Natalie Landon-Brace, Jose L Cadavid, Simon Latour, Ileana L Co, Darren Rodenhizer, Nancy T Li, Nila C Wu, Eryn Bugbee, Aleks Chebotarev, Ji Zhang, et al. An engineered patient-derived tumor organoid model that can be disassembled to study cellular responses in a graded 3d microenvironment. *Advanced Functional Materials*, 31(41):2105349, 2021.

[56] Rui-hua Xu, Helene Pelicano, Yan Zhou, Jennifer S Carew, Li Feng, Kapil N Bhalla, Michael J Keating, and Peng Huang. Inhibition of glycolysis in cancer cells: a novel strategy to overcome drug resistance associated with mitochondrial respiratory defect and hypoxia. *Cancer research*, 65(2):613–621, 2005.

[57] Weranja KB Ranasinghe, Lin Xiao, Suzana Kovac, Mike Chang, Carine Michiels, Damien Bolton, Arthur Shulkes, Graham S Baldwin, and Oneel Patel. The role of hypoxia-inducible factor 1α in determining the properties of castrate-resistant prostate cancers. *PloS one*, 8(1):e54251, 2013.

[58] EO Mosaad, KF Chambers, Katarzyna Futrega, JA Clements, and MR Doran. The microwell-mesh: A high-throughput 3d prostate cancer spheroid and drug-testing platform. *Scientific reports*, 8(1):1–12, 2018.

[59] LH Higgins, HG Withers, A Garbens, HD Love, L Magnoni, SW Hayward, and CD Moyes. Hypoxia and the metabolic phenotype of prostate cancer cells. *Biochimica et Biophysica Acta (BBA)-Bioenergetics*, 1787(12):1433–1443, 2009.

[60] Gail P Risbridger, Roxanne Toivanen, and Renea A Taylor. Preclinical models of prostate cancer: patient-derived xenografts, organoids, and other explant models. *Cold Spring Harbor perspectives in medicine*, 8(8):a030536, 2018.

[61] Julius S Horoszewicz, Susan S Leong, Elzbieta Kawinski, James P Karr, Hannah Rosenthal, T Ming Chu, Edwin A Mirand, and Gerald P Murphy. Lncap model of human prostatic carcinoma. *Cancer research*, 43(4):1809–1818, 1983.

[62] ATCC Thawing. Propagating, and cryopreserving protocol. Technical report, NCI-PBCF-HTB81 (DU 145), Prostate Carcinoma (ATCC® htb-81), Version 1.6, 2012.